Heliyon 6 (2020) e03655

Contents lists available at ScienceDirect

Heliyon

journal homepage: www.cell.com/heliyon

Research article

A novel hydrothermal synthesis of nanohydroxyapatite from eggshell-calcium-oxide precursors

Atiek Rostika Noviyanti [a,*], Nur Akbar [a], Yusi Deawati [a], Engela Evy Ernawati [a], Yoga Trianzar Malik [a], Retna Putri Fauzia [b], Risdiana [c]

[a] Physical-Inorganic Chemistry Laboratory, Department of Chemistry, Faculty of Mathematics and Natural Sciences, Universitas Padjadjaran, Jl. Raya Bandung-Sumedang Km. 21, Jatinangor, Sumedang, 45363, Indonesia
[b] Analytical Chemistry Laboratory, Department of Chemistry, Faculty of Mathematics and Natural Sciences, Universitas Padjadjaran, Jl. Raya Bandung-Sumedang Km. 21, Jatinangor, Sumedang, 45363, Indonesia
[c] Department of Physics, Faculty of Mathematics and Natural Sciences, Universitas Padjadjaran, Jl. Raya Bandung-Sumedang Km. 21, Jatinangor, Sumedang, 45363, Indonesia

ARTICLE INFO

Keywords:
Materials science
Nanotechnology
Hydroxyapatite
Hydrothermal
Eggshells

ABSTRACT

Hydroxyapatite (HA) is a material that has been widely applied to replace the damaged bone as a bone implant. Different types of HA have been successfully synthesized by a hydrothermal method based on calcium oxide (CaO) which was originated from chicken eggshells and diammonium hydrogen phosphate (DHP)/$(NH_4)_2HPO_4$ as their precursors. We present a novel approach to the hydrothermal synthesis of HA form eggshells as a new precursor via a one-step synthesis method. The influence of temperature was also observed to study the effect on the crystallinity, purity, and morphology of obtained HAs. The synthesis was carried out at two different temperatures, 200 °C (HA-200) and 230 °C (HA-230) for 48 h respectively. The structures, purities, and morphologies of hydroxyapatite were analyzed by X-ray Diffraction (XRD), Fourier Transform Infra-Red (FTIR), and Scanning Electron Microscopy- Energy Dispersive Spectroscopy (SEM-EDS), and Transmission electron microscopy (TEM). The XRD patterns show the HA main phase indicated the purity of 96.5% for HA-200 and 99.5% for HA-230. The TEM micrograph suggested a hexagonal-like of HA with an average particle size of 92.61 nm. Hexagonal-like of HAs are suitable for bone implants and further application.

1. Introduction

Hydroxyapatite (HA), $Ca_{10}(PO_4)_6(OH)_2$, is a mineral that has an important role in the component of hard tissue [1]. HA is a calcium phosphate-containing hydroxide that has a Ca/P ratio of 1.67. HA can help the growth of new bone without having to use fibrous tissue. HA can replace the damaged bone caused by the tumor, congenital diseases, and others as bone implants [2, 3]. HA is currently the most widely applied as materials in biomedical applications due to its stable chemical properties, composition, and crystal structure similar to human bone [4]. HA also can be the main-constituent materials of a composite for a bone implant such as gelatin/hydroxyapatite composite modified with osteoblast for bone bioengineering [5] and HA-based high-density polyethylene bio-composites [6].

Several studies have been performed to synthesize HA using natural materials as calcium sources such as coral, seaweed, and chicken eggshells [7, 8], shells [6], and starfish [2]. The chicken eggshells are a good source of calcium that was easily obtained than the other source of calcium. In addition, waste eggshells are abundant in Indonesia. The eggshells produced in a year are 138,956 tons [9], whilst the eggshells $CaCO_3$ content could have reached a percentage of 94% [10]. The chicken eggshells showed a suitable potential for the synthesis of high-quality hydroxyapatite as a good implant material [11]. Hence, the chicken eggshells potentially become a source of calcium in the synthesis of HA.

HA can be synthesized using various methods including solid phase reaction method [12], precipitation [13], and hydrothermal [2, 11]. Pei *et al.* [12] synthesized HA using $CaCl_2$ as a source of calcium by the solid-state reaction method at 775 °C. Yelten & Suat [13] synthesized HA from $Ca(OH)_2$ as a source of calcium by precipitation method. The extraction process and natural waste source in the HA synthesis have an effect on the critical properties of the HA such as Ca/P ratio, crystallinity

* Corresponding author.
E-mail address: atiek.noviyanti@unpad.ac.id (A.R. Noviyanti).

https://doi.org/10.1016/j.heliyon.2020.e03655
Received 9 January 2020; Received in revised form 9 March 2020; Accepted 20 March 2020

and phase assemblage, particle sizes, and morphology [14]. In the synthesis process, there are two phases: HA formation of $Ca(OH)_2$ and phosphoric acid at a temperature of 50–60 °C with a pH that must be controlled every last drop followed by a sintering process of HA synthesized at 900–1000 °C. Rodriguez-Lugo *et al.* [2] synthesized HA from CaO derived from starfish as a source of calcium and β-tricalcium phosphate by using the one-step hydrothermal method at 230 and 250 °C and produced homogeneous crystalline of HA. However other phases of HA were still observed.

The hydrothermal method can be deployed for a synthesis of high-crystalline and doped apatite-based materials [15, 16]. Thus, we utilise the method to provide good quality, purity, and high yield in HA synthesis. The method can be fruitful to acquire an excellent structural building of HA. Some of the advantages with this method are low cost, short reaction steps, low-temperature synthesis, simple method, and obtaining good quality of HA. This method is also associated with a low energy dissolution process, so it is easy to form pure and homogeneous crystalline HA and unique morphology at relatively low temperatures [17, 18].

Hydrothermally HA synthesis can be influenced by several factors, such as temperature, time, and pH during the synthesis process. From the set of results obtained in this research, it can be established that the best synthesis conditions for HAs are a temperature of 250 °C during a reaction time of 48 h. These parameters yielded the best characteristics of HA, including a more uniform size, greater amounts, homogeneity with a Ca/P ratio near stoichiometric, and a higher crystalline degree [19]. HA in various pH condition were successfully synthesized by hydrothermal method [20]. At high pH at 9, the form of HA will grow into spherical shape, meanwhile at lower pH up to 6, will grow into one-dimensional nanorods or two-dimensional nanoplates. Additionally, more complicated shapes, including three-dimensional microfibers, three-dimensional microtubes, and three-dimensional feathery are only obtained if the pH value decreases to 4.

Based on those studies, we conducted the HA synthesis via a one-step hydrothermal method using the variant source of CaO from chicken eggshell [2] and dissimilar phosphate source of DHP solution [9], more economically priced than β-tricalcium phosphate. The synthesis step reaction was noted in the following reaction **(1)**:

$$10CaO_{(s)} + 6(NH_4)_2HPO_{4(S)} + 4H2O_{(l)} \rightarrow Ca_{10}(PO_4)_6(OH)_{2(s)} + 12NH_4OH_{(aq)} \quad (1)$$

Meanwhile, the reaction underwent abasic pH between 9 and 10 to obtain a spherical shape for the application in the dental filling.

2. Experimental method

2.1. Conversion of $CaCO_3$ to CaO from chicken eggshell

Chicken eggshells were washed with water to remove the contaminants, then crushed by used planetary ball mill until 100 meshes. After being crushed, the material was calcined at 1000 °C for 5 h for the complete conversion of $CaCO_3$ to CaO. The phase composition of the material was characterized by XRF (Rigaku NEX CG).

2.2. Synthesis and characterization of HA

The synthesis was carried out at a different temperature of 200 °C (HA-200) and 230 °C (HA-230). CaO and DHP with the molar ratio of Ca/P = 1.67 were poured to distilled water (50mL). The mixture was then put into an autoclave 100mL and heated at 200 °C for 48 h. The obtained HA was filtered and washed with aquadest until pH = 7 to remove the NH_4OH and then dried at 110 °C for 2 h. The same procedure was repeated for the synthesis of HA at 230 °C. HA crystal structure identified by XRD (PANalytical X'PERT PRO seri PW 3040/x0) using CuK_α radiation at 2θ 5°–70°, the functional group of HA was confirmed by FTIR spectroscopies (PerkinElmer Spectrum 100). HA morphology and elemental mapping analysis were characterized by SEM-EDS (Jeol jsm-6360LA) and Transmission Electron Microscope/TEM (JEOL JEM-1400plus TEM Single tilt holder TEM Grid Cu 400 mesh).

3. Result and discussion

3.1. Calcination of chicken eggshells

At the temperature of 750 °C, $CaCO_3$ started to decompose into CaO, then completely decomposed at 1000 °C with the loss of ignition (LoI) of 45.96% due to the decomposition of chicken eggshells from $CaCO_3$ to CaO, as shown in reaction **(2)** [2]. The phase compositions of chicken eggshells after calcination at 1000 °C, are shown in Table 1.

$$CaCO_{3(s)} \overset{1000^\circ C}{\underset{\Delta}{\rightarrow}} CaO_{(s)} + CO_{2(g)} \quad (2)$$

The CaO content was 97.80%, which was then used to calculate the molar ratio a Ca source of the HA formation reaction with DHP as a phosphate source.

3.2. Structural characterization of HA by XRD

The XRD patterns of HA-200 and HA-230 are shown in Figure 1. The main peak of HAs was indicated at around 2θ ~31°. The portlandite phase was observed at 2θ ~17.2°.

The purity of HA-200 and HA-230 was 96.5% and 99.5% with 3.5% and 0.5% secondary phase *portlandite* ($Ca(OH)_2$) respectively. This fact suggests that the reaction temperature can affect *portlandite* $Ca(OH)_2$ content. The lower reaction temperatures produced more *portlandite*. The higher the reaction temperature, the higher a reaction rate between $Ca(OH)_2$ and DHP, the more HA was produced. HA-200 and HA-230 have a hexagonal structure with space group *P63/m* with slightly different lattice parameter as shown in Table 2.

Different temperatures of synthesis were also affected to the crystal size and crystallinity of HA. The crystallinity of synthesizing HA was calculated from the XRD data using the Debye-Scherrer equation, Eq. (3) below [19]:

$$Xc = 100 \times \left(I_{300} - V_{112/300}\right)/I_{300} \quad (3)$$

where I_{300} is the intensity of the diffraction peak at the (300), $V_{112/300}$ is the intensity of the (112) and (300). The crystallinity of HA-230 is 72.76%, meanwhile, HA-200 is 67.23%. This phenomenon complies with another study we found demonstrating that the increase in processing temperature had a great effect on the particle size and crystal structure of HA. The low temperature (−10 °C) showed inhabitation of the HA growth in c-direction and low crystallinity which was confirmed using XRD and electron diffraction pattern of TEM [21, 22].

Higher temperature elevates the evaporation rate of the solvent, thus accelerating the crystal growth rate. The disparate temperatures produce different amounts of crystals. Colder solutions contract, adjusting atoms in the HA structure assemble forcing bonds to develop, engaging impurities in the structure simultaneously. These impurities subsequently interrupt the crystal pattern, supporting the formation of a larger number of smaller crystals. In warmer temperatures, the distance between molecules is wider, which allows crystals to form larger, purer shapes at a much more uniform rate than can occur in colder temperatures implying that the crystallinity would be larger by deploying a higher temperature [23].

Table 1. Phase Composition of chicken eggshells after calcination.

Component	Composition (%)
CaO	97.80
P_2O_5	0.29
Fe_2O_3	0.01
SiO_2	0.16
K_2O	0.18
SO_3	0.16
Al_2O_3	0.18
MgO	1.17

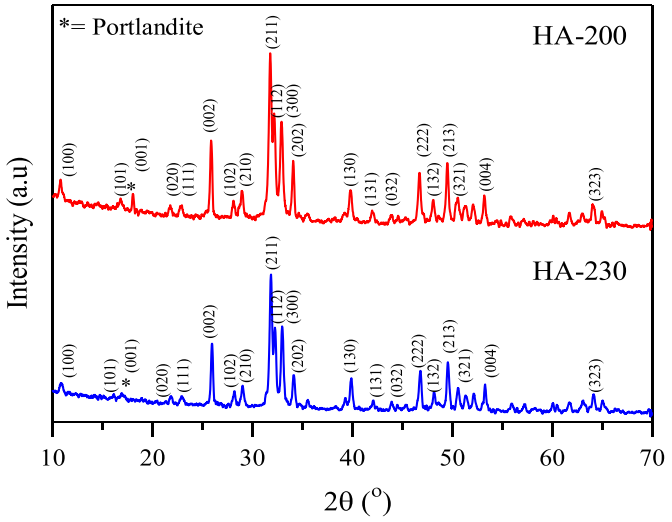

Figure 1. XRD pattern of HA-200 and HA-230.

3.3. FTIR characterization of HA

To confirm the functional groups of two different types of HA, FTIR spectroscopy analysis was also conducted. Figure 2 shows the FTIR spectra of HA-200 (top) and HA-230 (bottom). The HA-200 showed the stretching of the P–O bond from the PO_4^{3-} at 566, 962, and 1025 cm^{-1}. Bending of the P–O bond from the PO_4^{3-} of HA was observed at 602 cm^{-1}, the O–H stretching and bending appeared at 3571 and 632 cm^{-1}, respectively [2]. The formation of carbonated apatite with B-type substitution (tetrahedral positions) was is indicated by the presence of a peak at 1401cm^{-1} (H–O–H) [11]. Overall the FTIR HA-200 and HA-230 spectra were very similar. This implies that the difference in the temperature of synthesis does not influence the dissimilarity of HA functional groups. The functional groups detected on HA-200 and HA-230 are shown in Table 3. We can perceive that HA-200 forms a broader band at ~1000 cm^{-1} than the HA-230 spectrum which indicates a difference of their PO_4^{3-} asymmetric stretching.

The HA formed in this study is slightly different from the HA obtained from a previous paper [2] which exhibited five of the nine bands of the PO_4 ion and one corresponding to the OH ions. The differences in source precursors (in this study, DHP was used as a phosphate source, while reference studies were used β-TCP), might cause small differences in

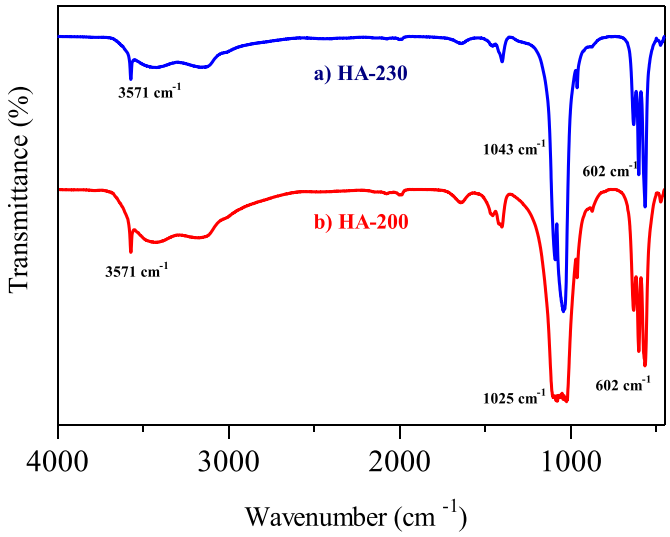

Figure 2. The FTIR spectra of HA-200 (a) and HA-230 (b).

shifts and intensities for P–O vibrational modes in PO_4 groups. The bands emanate from 910 cm^{-1} and 715 cm^{-1} which correlates to the P–O vibration mode of the PO_4 ion. Furthermore, the formation of a band localized at 3650 cm^{-1}, which perhaps due to the emergence of HO hydroxyls, suggested the $Ca(OH)_2$ formation. It would also be feasible to characterize a band due to the H–O–H mode, which was related to moisture located at 3460 cm^{-1} which may also be distinct the HA spectrum in this study.

3.4. Morphology characterization of HA using SEM-EDS

Both the HA-200 and HA-230 morphologies are agglomerates with spherical and porous particle shapes. The morphology SEM of HA-230 is shown in Figure 3 (b) denoted a more homogenous flock than the HA-200 (Figure 3. (a)). It suggests that the increase in temperature allows the size of the particles to grow larger (in terms of diameter) and the form homogeneity is quite high [2]. Higher synthesis temperatures will produce particles with a more regular form because at higher temperatures they have higher crystallinity [24].

The regular form could be perfectly suitable for bone implantation [24]. It is known that the surface shape and texture of implants play a significant role in regulating tissue response and cell activities [25]. Hulbert et al. [26] studied the tissue reaction of three ceramics with porous and non-porous structures in soft and live tissue. The results showed that tissue around porous implants healed quickly.

Semi-quantitative analysis of EDS shows that the Ca/P molar ratio of HA-200 is 2.44 and the Ca/P molar ratio of HA-230 is 2.29. Table 4 shows that calcium contents in HA-200 were slightly higher (47.02%) than HA-230 (45.98%) while the phosphor contents were lower that prompted a larger ratio of Ca/P in HA-200 than in HA-230. This result exceeds the Ca/P molar ratio of stoichiometric HA. This is due to the possibility of contamination of carbonate (CO_3^{2-}) as shown in FTIR spectra from the air which can react with HA, causing a decrease in PO_4^{3-}. In addition, it can be caused because the HA phase produced is not 100% but there is a by-product, $Ca(OH)_2$ as shown in the XRD result so that it changed the

Table 2. The lattice parameter, crystallite size and percentage of crystallinity of HA-200 and HA-230.

Samples	Lattice parameter		Crystallite size (nm)	Crystallinity (%)
	a = b (Å)	c = (Å)		
HA-200	9.4155(8)	6.8786(3)	24.57	67.23
HA-230	9.4168(1)	6.8794(1)	35.28	72.76

Table 3. Comparison of FTIR spectra of HA-200 and HA-230.

No	Functional Groups	Wavenumber at 200 °C (cm^{-1})	Wavenumber at 230 °C (cm^{-1})
1	PO_4^{3-} stretching	566 and 962	565 and 962
2	PO_4^{3-} asymmetric stretching	1025	1043
3	PO_4^{3-} asymmetric bending	602	602
4	Free O–H stretching	3571	3571
5	H–O–H	3422	3422
6	O–H bending	632	632
7	CO_3^{2-}	1403	1401

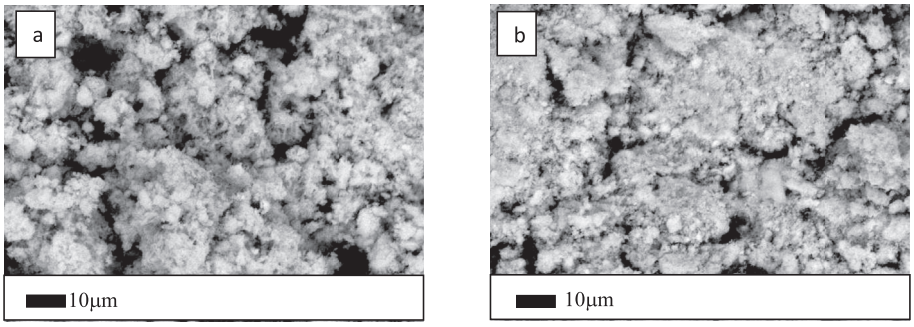

Figure 3. SEM image of HA-200 (a) and HA-230 (b) surface.

Table 4. Chemical Composition of HA-200 and HA-230 was analized by using SEM.

Element	Content (%)	
	HA-200	HA-230
Ca	47.02	45.98
P	14.93	15.56
O	38.05	38.45

molar ratio of Ca/P from both HA-200 and HA-230. To confirm the difference of Ca/P ratio in both HA-200 and HA-230, the elemental mapping was generated as shown in Figure 4.

Elementary mapping analysis is performed to determine the distribution of elements in HA. The colors besides the SEM morphology express the intensity of the distribution of certain elements. The color order from top to bottom indicates a decrease in the distribution of these elements at the specified hydroxyapatite spot. For example, in HA-200 the highest oxygen distribution is in the middle to the bottom (red) and appears to decrease in the left side (blue). Oxygen and phosphorus distribution in HA230 is higher than that HA200, while the distribution of calcium is almost the same in HA -200 and HA-230 The analysis of oxygen, calcium and phosphorus mapping on both HA supports the results of the XRF analysis which confirms the Ca/P ratio at HA-230 is lower than the Ca/P ratio at HA-200.

The grain shape of HA particles was confirmed using TEM as shown in Figure 5. The micrograph indicated hexagonal-like-to-round shapes of HA. The average particle size is 92.61 nm with the largest to the lowest size denoted 128.77 nm and 63.89 nm respectively. We found that the agglomeration occurred at HA-230 which shows larger particles than HA-200. This corroborates the evidence of higher crystallite size (35.28 nm) and crystallinity (72.76%) of HA-230.

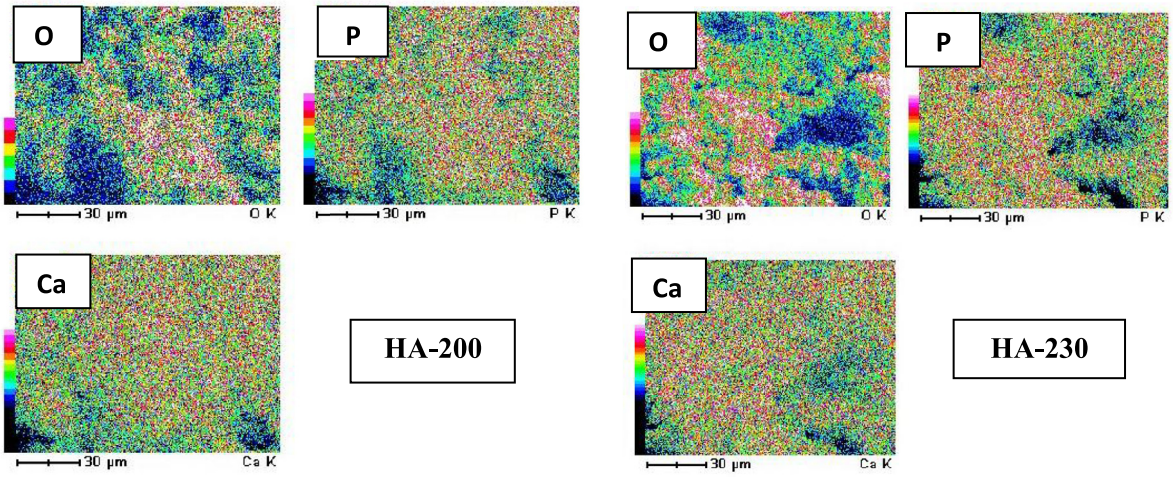

Figure 4. The elemental mapping of oxygen (O), calcium (Ca), and phosphor (P), respectively in HA-200 and HA-230. The distribution of each element is shown in a different colour.

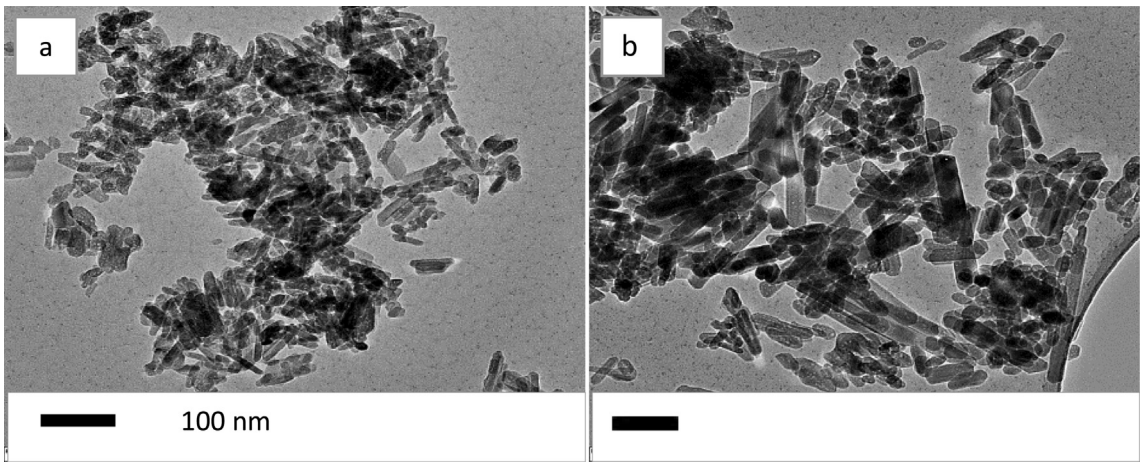

Figure 5. TEM micrograph of HA-200 (a) and HA-230 (b) surface.

4. Conclusion

HA-200 and HA-230 were successfully synthesized using the hydrothermal method from the chicken-eggshells calcium oxide. It can be concluded that the hydrothermal synthesis method of HA performed excellent results with a one-step synthesis using eggshells source of calcium as the precursor. HA-230 demonstrated better results with a lower Ca/P ratio (2.29) other than HA-200 with Ca/P ratio (2.44). The XRD resulted in an additional peak to HA-200 which corresponded to $Ca(OH)_2$ impurities. This suggested that HA-230 had a better structure than that HA-200. Therefore, HA-230 is considered most appropriate as a biomaterial for implantation due to the proximity of the structural and composition to the commercial HA. In addition, to obtain HA with 92 nm of average particle size, the novel-one-step synthesis of HA is also suggested. The hexagonal-like structure would be considered suitable for biomaterial applications such as a bone implant. The developments of chicken eggshells are expected to be prevalently applicable in miscellaneous implementation.

Declarations

Author contribution statement

Atiek Rostika Noviyanti: Conceived and designed the experiments.
Nur Akbar, Retna Fauzia Putri: Performed the experiments.
Yusi Deawati, Yoga Trianzar Malik: Analyzed and interpreted the data; Wrote the paper. Engela Evi Ernawati: Contributed reagents, materials, analysis tools or data.
Risdiana: Analyzed and interpreted the data.

Funding statement

This work was supported by the Directorate General of Higher Education, Ministry of Research and Technology, Republic of Indonesia through PDUPT (Penelitian Dasar Unggulan Perguruan Tinggi) No. 2789/UN6.D/LT/2019 and Funding for Master Thesis No. 2894/UN6.D/LT/2019.

Competing interest statement

The authors declare no conflict of interest.

Additional information

No additional information is available for this paper.

Acknowledgements

The authors would like provide a sincere gratitude to Delft University (Faculty of Applied Sciences), The Netherlands for the technical support on TEM measurement.

References

[1] C.R. Kothapalli, M. Wei, R.Z. Legeros, M.T. Shaw, Influence of temperature and aging time on HA synthesized by hydrothermal method, J. Mater. Sci. Mater. Med. 16 (2005) 441–446.
[2] V. Rodriguez-Lugo, Salinas-Rodriguez, R.A. Vazquez, HydroxyapatiCte synthesis from a starfish and β-tricalcium phosphate using a hydrothermal method, Royal Soc. Chem. 7 (2017) 7631–7639.
[3] A.H. Dewi, I.D. Ana, The use of hydroxyapatite bone substitute grafting for alveolar ridge preservation, sinus augmentation , and periodontal bone defect: a systematic review, Heliyon (2018) (May).
[4] Ming Ni, D. Ratner Buddy, Nacre surface transformation to hydroxyapatite in a phosphate buffer solution, Biomaterials 24 (23) (2003) 4323–4331.
[5] N. Yadav, P. Srivastava, In vitro studies on gelatin/hydroxyapatite composite modi fi ed with osteoblast for bone bioengineering, Heliyon 5 (2019) (December 2018).
[6] I. Oluwole, O. Ganiu, A. Adesoji, Heliyon Structural performance of poultry eggshell derived hydroxyapatite based high density polyethylene bio-composites, Heliyon 5 (2019) (February).
[7] G. Saraswathy, S. Pal, C. Rose, Sastry, A novel bio-inorganic bone implant containing deglued bone, chitosan and gelatin, Bull. Mater. Sci. 24 (4) (2001) 415–420.
[8] Y. Azis, Hadi N. Novesar Syukri, Facile synthesis of hydroxyapatite particles from cockle shells (anadaragranosa) by hydrothermal method, Orient, J. Chem. 31 (2) (2015) 1–7.
[9] Nurdiman Maman, Ramadhany Aslila, Livestocks and Animal Health Statistics, Direktorat Jenderal Peternakan dan Kesehatan Hewan Kementerian Pertanian RI, Jakarta, 2018. https://ditjenpkh.pertanian.go.id/userfiles/File/Buku_Statistik_2018_Final_ebook.pdf?time=1543210844103.
[10] E.M. Rivera, A. Miguel, B. Witold, M.C. Victor, J.R. Diaz-Estrada, R. Hernandez, J.R. Rodriguez, Synthesis of hydroxyapatite from eggshells, Mater. Lett. 41 (1999) 128–134.
[11] G. Gergely, F. Wéber, I. Lukács, A.L. Tóth, Z.E. Horváth, J. Mihály, C. Balázsi, Preparation and Characterization of hydroxyapatite from eggshell, Ceram. Int. 36 (2) (2010) 803–806.
[12] L. Pei, T. Takuya, D. Aaron, S. Martin, Synthesis of calcium chlorapatite nanoparticles and nanorods via a mechanically-induced solid-state displacement reaction and subsequent heat treatment, Cermics Int. 43 (14) (2017) 11410–11414.
[13] A. Yelten, Y. Suat, Various parameters affecting the synthesis of the hydroxyapatite powders by the wet chemical precipitation technique, Proceedings 3 (2016) 2869–2876.
[14] N.A.S.M. Pu'ad, P. Koshy, H.Z. Abdullah, M.I. Idris, T.C. Lee, Syntheses of hydroxyapatite from natural sources, Heliyon 5 (2019) (October 2018).
[15] Y.T. Malik, A.R. Noviyanti, N. Akbar, I. Hastiawan, T. Saragi, Risdiana, Structure, chemical stability and magnetic properties of lanthanum silicate oxide apatite synthesized by hydrothermal method, Mater. Sci. Forum 966 (2019) 415–421 (August 2019).
[16] A.R. Noviyanti, N. Akbar, I. Hastiawan, I. Rahayu, Haryono, Y.T. Malik, Risdiana, Bi-doping effect on the conductivity of lanthanum silicate apatite, Mater. Sci. Forum 966 (2019) 451–455.
[17] T. Goto, Y.I. Kim, K. Kikuta, C. Ohtsuki, Hydrothermal synthesis of composites of well- crystallized hydroxyapatite and poly (vinyl alcohol) hydrogel, Mater. Sci. Eng. C 32 (2012) 397–403.

[18] J.K. Han, Y.S. Ho, S. Fumio, T.L. Byong, Synthesis of high purity nano-sized hydroxyapatite powder by microwave-hydrothermal method, Mater. Chem. Phys. 99 (2006) 235–239.
[19] J.S. Earl, D.J. Wood, S.J. Milne, Hydrothermal synthesis of hydroxyapatite, J. Phys. Conf. 26 (2006) 268–271.
[20] M. Sadat-Shojai, T.K. Mohammad, J. Ahmad, Hydrothermal processing of hydroxyapatite nanoparticles-A taguchi experimental design approach, J. Cryst. Growth 361 (2012) 73–84.
[21] S. Dey, M. Das, V.K. Balla, Effect of hydroxyapatite particle size, morphology, and crystallinity on proliferation of colon cancer HCT116 cells, Mater. Sci. Eng. C 39 (2014) 336–339.
[22] H. Elhendawi, R.M. Felfel, B.M.A. El-hady, F.M. Reicha, Effect of synthesis temperature on the crystallization and growth of in situ prepared nanohydroxyapatite in chitosan matrix, Hindawi (2014).
[23] G. Wypych, Parameters of Crystallization, Handbook of Nucleating Agents, Chemtec Publishing, Canada, 2015, pp. 53–59, 2006.
[24] X.Y. Pang, X. Bao, Influence of temperature, ripening time, and calcination on the morphology and crystallinity of hydroxyapatite nanoparticles, J. Eur. Ceramic Soc. 23 (2003) 1697–1704.
[25] S.C. Chao, W. Ming-Jia, P. Nai-Su, Y. Shiow-Kang, Preparation and characterization of gelatin- hydroxyapatite composite microspheres for hard tissue repair, Mater. Sci. Eng. C 57 (2015) 113–122.
[26] S.F. Hulbert, S.J. Morrison, J.J. Klawitter, Tisuue reaction to three ceramics of porous and non- porous structures, J. Biomed. Mater. Res. 6 (1972) 347–374.